https://doi.org/10.5194/egusphere-2026-613
Preprint. Discussion started: 16 March 2026

Linking individual-based forest modelling with a radar simulator for determining forest structure and biomass

Leonard Grohmann[1], Lea Albrecht[2], Kostas Papathanassiou[2], and Andreas Huth[1,3,4]

[1]Dept. of Ecological Modelling, Helmholtz Centre for Environmental Research - UFZ, Leipzig,Germany
[2]German Aerospace Center - DLR, Oberpfaffenhofen, Germany
[3]Institute of Environmental Systems Research, Osnabrück University, Osnabrück, Germany
[4]Centre for Integrative Biodiversity Research - iDiv, Leipzig, Germany

Correspondence: Leonard Grohmann (leonard.grohmann@ufz.de) and Andreas Huth (andreas.huth@ufz.de)

Abstract. Mapping forest structure, critical for assessing carbon stocks and fluxes, remains challenging with remote sensing. We propose a novel framework linking an individual-based forest model (FORMIND), which generates explicit 3D forest structures and dynamics, with a radar simulator (here used for TanDEM-X). We investigate radar coherence from simulated forests to predict aboveground biomass (AGB) across varying spatial scales, measurement noise levels, and successional stages. The framework is applied to the Barro Colorado Island (BCI) tropical forest, where we evaluate simulated coherence against TanDEM-X observations and invert canopy height, comparing the results with airborne laser scanning (ALS) data. Results indicate a positive link between forest structure and interferometric patterns, with AGB prediction showing a clear dependence on spatial resolution. This novel approach offers a pathway to map forest structure by combining broad radar data coverage with an ecologically explicit forest model.

1 Introduction

Earth's forests are foundational elements of the global carbon balance, with carbon stock estimates ranging from 500-900 GT (Pan et al., 2011; Harris et al., 2021), while contributing approximately 3 GT of annual net carbon sequestration (Mo et al., 2023; Cherrington et al., 2024). Global forests are heterogeneous in both their carbon stocks and fluxes (Zhao et al., 2020; Bauer et al., 2021). Under anthropogenic and climatic pressures, the world's forests are changing rapidly. Mapping current carbon stocks and fluxes is a widespread effort to reduce uncertainties, support decision-making, and plan conservation. Canopy height has emerged as a key predictor for forest biomass estimation, demonstrated through both field-based studies (Knapp et al., 2020) and remote sensing approaches (Choi et al., 2023; Lang et al., 2023). However, this important structural metric alone is insufficient, as other forest structural properties are needed for accurately characterizing carbon fluxes and local forest dynamics (Rödig et al., 2018). The successional dynamics, disturbances, and the forest's response to them often depend on local conditions (Rödig et al., 2019). This introduces large spatial variability to global forests and their structure.

For capturing forest structure, key for biomass stocks and carbon fluxes (Rödig et al., 2018), current remote sensing approaches face limitations. While LiDAR (ICESat-2 GEDI) provides global coverage (Dubayah et al., 2022), its point measurements create challenges for upscaling from tree to forest scale (Burns et al., 2024; Lang et al., 2023). The TerraSAR-X add-on

https://doi.org/10.5194/egusphere-2026-613
Preprint. Discussion started: 16 March 2026

for Digital Elevation Measurement (TanDEM-X) radar coherence offers continuous coverage with high spatiotemporal resolution (e.g., 10 m–100 m), but existing applications focus primarily on height mapping rather than structural characterization (Choi et al., 2023; Zhang et al., 2025). Individual-based forest models can bridge these knowledge gaps by providing relations between different forest attributes and a mechanistic understanding of forest structure (Bauer et al., 2021), therefore offering the possibility of a detailed radar analysis.

Here, we propose a new approach to integrate forest structure in assessing TanDEM-X radar measurements by directly including radar simulations into a forest model. Analyses of Airborne Laser Scanning (ALS) data showed the feasibility of deriving local structural composition from individual-based forest models (Knapp et al., 2020). Utilizing a region-specific FORMIND version (Rödig et al., 2019), canopy structures can be linked to radar observables such as the X-band coherence from the TanDEM-X mission by applying interferometry (Treuhaft et al., 1996). This fusion of detailed ecological process modeling with remote sensing data offers a powerful pathway to better understand and predict forest structural properties across different spatial scales.

Our results demonstrate the capability to link forest radar coherence to forest structural properties. We investigate the predictive power for aboveground biomass (AGB) across spatial scales, under different measurement noise scenarios, and covering different successional stages. Subsequently, at our tropical forest case study site, Barro Colorado Island (BCI), we evaluate the model's performance by comparing simulated interferometry with radar observations and inverting forest heights, validating these estimates against ALS data.

In this study, we investigate three main research questions:

1. How can forest modeling enhance radar coherence interpretation for characterizing forest structure and its influence on aboveground biomass?
2. How well do radar simulations reproduce observed patterns in tropical forests?
3. How effectively can forest canopy height be retrieved from X-band radar coherence using an inversion of a radar simulator, and how do estimates compare with airborne laser scanning (ALS) results?

2 Material and Methods

2.1 Study site

For this study we use a tropical forest as reference site. This site is located at Barro Colorado Island (BCI, approx. 9.15°N, 79.85°W) and includes a 50 ha plot of mature semi-deciduous Neotropical forest with a high biodiversity of around 300 tree species (Condit et al., 2012a). The climate is characterized by a dry season and geographic isolation. The forest is documented through the Smithsonian Forest Inventory (Condit et al., 2012a), offering about 40 years of continuous inventory data. The forest is dominated by canopy heights of 30-40 meters, with emergent trees occasionally reaching 45-50 meters (Hubbell, 2013). The forest maintains an aboveground biomass (AGB) of approximately 280 $\mathrm{t\,ha^{-1}}$ on average (Chave et al., 2003;

https://doi.org/10.5194/egusphere-2026-613
Preprint. Discussion started: 16 March 2026

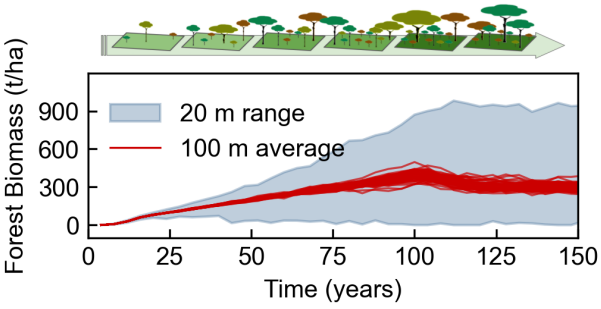

Figure 1. Successional dynamics of forest growth. Development of local AGB of the tropical forest in BCI. Different functional tree types with distinct growth strategies drive the succession from bare ground to mature forest (Knapp et al., 2020). The variability on the local scale - especially in older stands with complex multi-layered structures - is captured by the individual-based model FORMIND (Fischer et al., 2016).

Mascaro et al., 2010), typical for old-growth forests in the Americas. Due to its large size, it is a valuable reference site for projecting forest dynamics to other tropical forests, as has been demonstrated by Feeley et al. (2011). We analyzed forest structure from the 2012 inventory by using tree diameter at breast height (DBH) and position data (Condit et al., 2012b). In addition, we utilized airborne laser scanning (ALS) data (Meyer et al., 2013) to validate our model's predictions.

2.2 Individual-Based Forest Model

The forest model FORMIND simulates tree growth and forest dynamics through a mechanistic approach (Fischer et al., 2016). Individual trees are represented with their specific sizes, positions, and plant functional types, competing for light, water, and space. The model incorporates key ecological processes including size-dependent growth, carbon production and storage, competition, mortality, seed dispersal, and regeneration at the individual tree level.

The forest model FORMIND has been extensively validated across diverse forest ecosystems worldwide (Tietjen and Huth, 2006; Armstrong et al., 2018). Its applications range from analyzing biodiversity patterns and species coexistence to assessing forest resilience under climate change and anthropogenic disturbances (Köhler and Huth, 1998; Hiltner et al., 2021). The model's predictions have contributed to understanding long-term forest succession, carbon storage dynamics, and ecosystem responses to environmental change (Henniger et al., 2023; Fischer et al., 2024). Figure 1 illustrates the dynamics of forest succession simulated by FORMIND for the study site at BCI.

This individual-based approach enables the simulation of different structural forest compositions at a resolution of 20 m, together with forest properties such as the height of the local largest tree (for a Canopy Height Model CHM), stand age, AGB, and carbon fluxes. These forest attributes can be also used as inputs for radar backscatter modeling.

https://doi.org/10.5194/egusphere-2026-613
Preprint. Discussion started: 16 March 2026

2.3 TanDEM-X radar coherence

The TanDEM-X mission operates as a bistatic X-band radar system ($\lambda = 3.1\,\mathrm{cm}$) with two satellites, providing Earth surface measurements (Zink et al., 2007). Leaves, twigs, and branches are effective scatterers at this wavelength and interaction with the canopy structure makes the backscatter signal valuable for forest investigation. We analyze TanDEM-X datasets, where coherence amplitude serves as a main metric for interferometric analysis (Papathanassiou and Cloude, 2001). The orbital acquisition parameters for our study site can be found in Appendix D (Zink et al., 2007). These influence the interferometric measurements and the azimuth and range resolution of it.

The coherence γ is defined as the normalized complex cross-correlation between the two acquisitions s_1 and s_2, where s_1 and s_2 represent the complex radar signals received from the same ground area by each of the two TanDEM-X satellites:

$$\gamma = |\gamma| \exp(j\phi) = \frac{< s_1 s_2^* >}{< s_1 s_1^* >< s_2 s_2^* >} \tag{1}$$

Coherence is composed of amplitude and phase components $\gamma = |\gamma| \exp(j\phi)$ and is affected by weather and atmospheric effects, such as the changing of dielectrical properties of leaves caused by rain events. The changing orbital constellations of the TanDEM-X mission result in varying baselines, which in turn modify the acquisition properties and affect the measurements.

The interferometric measurements depend on the vertical wavenumber κ_z, which is influenced by the system parameters: wavelength λ, azimuth angle θ, and baseline angle difference $\Delta\theta$ (Zink et al., 2007). The ground beneath the vegetation of height h_v can be captured by a digital elevation model (DEM) and is incorporated into the geometry of acquisition by the ground phase ϕ_0 and the observation angle θ through the vertical wavenumber κ_z:

$$\kappa_z = \frac{2\pi\Delta\theta}{\lambda \sin\theta} \tag{2}$$

Therefore, the vertical wavenumber varies locally with incidence angle and acquisition geometry (DEM-corrected). The phase component $\phi \in [0, 2\pi]$ relates to the average scatterer center height via $h_\phi = \phi/\kappa_z$ through the interferometric wavenumber κ_z and the normalized amplitude $|\gamma| \in [0, 1]$ defines the amount of decorrelation between the two acquisitions. This decorrelation can be approximated by three factors: systematic errors (γ_{sys} - influenced by acquisition parameters and measurement noise), volumetric decorrelation (γ_{veg} - depending on canopy structure), and temporal decorrelation (γ_{temp} - negligible in simultaneous bistatic acquisitions) (Bamler and Hartl, 1998).

2.4 Integrating forest structure and radar coherence

Radar signals interact with vegetation through scattering that depends on the structure of the forest canopy. The relationship between vertical vegetation structure and radar coherence is modeled by considering the signal's propagation through the different vegetation layers, where the signal is attenuated by the density of random scatterers ρ - resolved by depth z - as it travels downward through the canopy. Following Treuhaft et al. (1996), the coherence γ can be expressed as:

https://doi.org/10.5194/egusphere-2026-613
Preprint. Discussion started: 16 March 2026

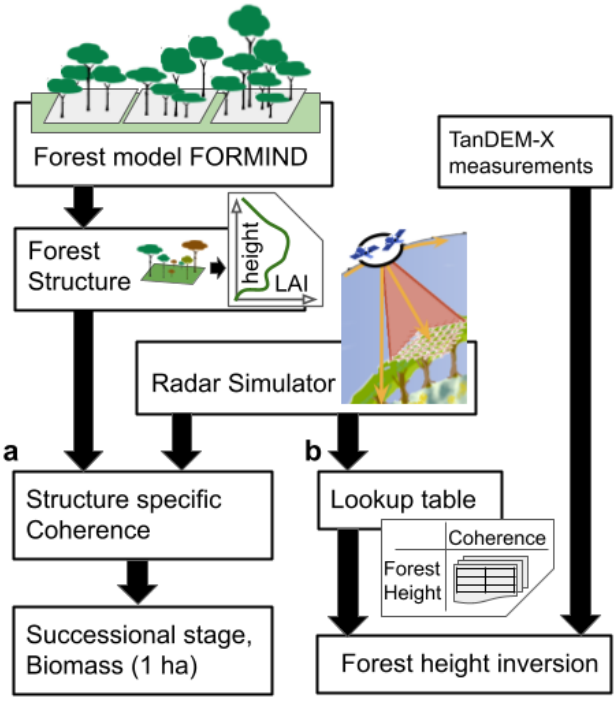

Figure 2. Forest model - radar integration framework. (a) predicting biomass from coherence based on local forest structure, (b) forest height inversion

$$\gamma = \exp(j\phi_0)\frac{\int \rho(z)\exp(j\kappa_z z)\,\mathrm{d}z}{\int \rho(z)\mathrm{d}z} \tag{3}$$

For X-band radar, we utilize the vertical distribution of the Leaf Area Index (LAI_i, LAI-profile) of individual trees i to model the vertical profile of the backscatterers.

$$\rho(z) = \sum_i \mathrm{LAI}_i(z) \tag{4}$$

The forest structure expressed as LAI distribution over height is then used to model radar backscattering on patch-scale ($20\,\mathrm{m} \times 20\,\mathrm{m}$). The attenuation of the signal with depth $\exp(-\frac{2\sigma h_v}{\cos\theta})$ is parameterized by the exponential attenuation factor σ and also depends on the incidence angle θ (Papathanassiou and Cloude, 2001).

We developed a radar simulator based on the Random Volume over Ground (RVoG) backscattering model (Treuhaft et al., 1996). Figure 2 shows the workflow for the analysis of this study. Forest structure can be sourced from either ecological model simulations or from field inventories. TanDEM-X coherence measurements and acquisition parameters (cf. Appendix D) are also used for this study.

https://doi.org/10.5194/egusphere-2026-613
Preprint. Discussion started: 16 March 2026

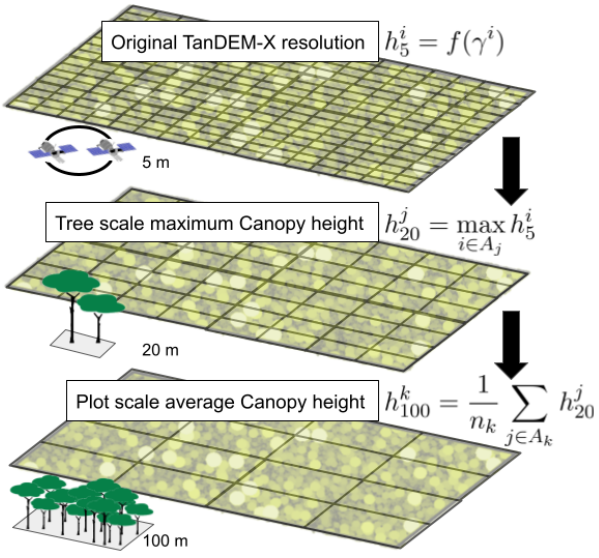

Figure 3. Canopy height aggregation process across spatial scales: Starting from TanDEM-X's 5-meter resolution coherence measurement cell i we inverted heights (h_5^i), max-sampling captures the largest tree at 20-meter at patch j (h_{20}^j), and mean-sampling is applied for 100-meter scale at plot k (h_{100}^k).

Our study includes two analyses: **(a)** Predicting biomass from coherence across forest successional stages modeled by FORMIND. **(b)** Inverting forest height from TanDEM-X coherence.

The former analysis incorporates the explicit forest structure and coherence based thereon, while the latter employs a generalized forest strucural profile to relate coherence to height.

2.5 Biomass prediction from radar coherence

Individual-based forest models enable the simulation of small scale forest structure, including LAI-profiles matching LiDAR energy return profiles (Knapp et al., 2020). We simulated 100 ha of natural growth from bare ground for 500 years using the FORMIND model parameterized for tropical forest in Panama (Knapp et al., 2020). These individual-tree based simulations span the full range of successional stages, biomass stocks and structural composition, providing a diverse set of forest states.

For each individual forest state at 20 m resolution, we used the unique LAI-profile to simulate X-band coherence amplitude, cf. Fig. 2(a). We then tested how well the coherence amplitude could predict forest biomass at different spatial scales and including different noise levels. At the 20 m scale, we tested a linear regression model using coherence amplitude $|\gamma|$ as a predictor for forest biomass. At the 100 m scale, we aggregated the coherence values at $20\,\mathrm{m} \times 20\,\mathrm{m}$ and tested three models: (1) a linear model with mean coherence amplitude, (2) a linear model with the standard deviation of coherence amplitudes, capturing local coherence variability, and (3) a bilinear model combining both mean and standard deviation of the normalized coherence amplitude. The regression models are tested using least-squares regression and are provided in more detail in Appendix B.

https://doi.org/10.5194/egusphere-2026-613
Preprint. Discussion started: 16 March 2026

To account for real-world measurement uncertainties in radar coherence, we introduced a decorrelation term to our coherence model:

$$\gamma_{sys} = \exp(-\sigma_{\mathcal{N}} Z)^2 \tag{5}$$

with Gaussian weights $Z \sim \mathcal{N}(0,1)$ at two levels, $\sigma_{\mathcal{N}} = 10\%$ and 20%. This yields an expected mean system-level decorrelation of $\hat{\gamma}_{sys} \approx 1/\sqrt{1+2\sigma_{\mathcal{N}}^2} \approx 0.96$ for $\sigma_{\mathcal{N}} = 20\%$. This noise model implies log-normal multiplicative decorrelation and is acquisition-independent; it represents the combined effects of measurement errors and atmospheric variations that can affect real TanDEM-X acquisitions. The corresponding multiplicative variance amounts to $(\gamma_{sys}) = \sqrt{1+2\sigma_{\mathcal{N}}^2} - \frac{1}{1+\sigma_{\mathcal{N}^2}} \approx 0.045$.

2.6 Forest Height Inversion

We developed a second method to estimate forest height (at the scale of 1 ha) from radar measurements. For this we used forest inventory data for the tropical forest at BCI.

There we explicitly assume that the scatterers are equally distributed (over height) in the forest and there is only a decay of the radar backscattering signal with depth. Using our radar simulator we can estimate the resulting coherence amplitude for each $5\,\mathrm{m} \times 5\,\mathrm{m}$ plot. Thus the obtained coherence depends only on the local forest (based on the largest tree at $5\,\mathrm{m} \times 5\,\mathrm{m}$) and acquisition parameters.

Our first height product (P_1) relates coherence amplitude to forest height. Coherence amplitude is calculated as in Eq. 3 for the profiles $\rho(z) = \exp(-\frac{2\sigma h_v z}{\cos\theta})$, $\sigma = 0.02$, creating a lookup-table for inversion at the scale of $5\,\mathrm{m} \times 5\,\mathrm{m}$ (Treuhaft and Siqueira, 2000).

The second product extends this lookup table by incorporating the phase information, averaging this amplitude-derived height with the phase-derived height $h_\phi = \phi/\kappa_z$ ($P_2 = \mathrm{mean}(P_1, h_\phi)$). Both the inversion of amplitude and of phase use acquisition- and pixel-specific κ_z.

Forest properties exhibit scale-dependent relationships with remote sensing metrics (Knapp et al., 2018). Spatial aggregation can improve prediction performance by averaging out local variations. Balancing these scale-dependent trade-offs, we implement a multi-scale aggregation strategy that preserves dominant structural features while achieving robust statistical properties. TanDEM-X's native resolution is defined in azimuth and range directions, varying across different acquisitions. Here, these approximately translate to a scale of 5 m at which forest height can be resolved (h_5). This small scale is where potential measurement noise can be effectively reduced (Papathanassiou and Cloude, 2001). We apply max-sampling of heights h_5 measured at the scale of 5 m to capture the largest trees in each 20 m cell (h_{20}), similar to Lorey height weighting (Lorey, 1887). Finally we average the obtained forest height h_{20} at 20 m resolution for 100 m plots, getting h_{100}. The aggregation process is illustrated in Figure 3. We validate both height inversion products P_1, P_2 against ALS-derived forest heights (Meyer et al., 2013) at the hectare scale.

https://doi.org/10.5194/egusphere-2026-613
Preprint. Discussion started: 16 March 2026

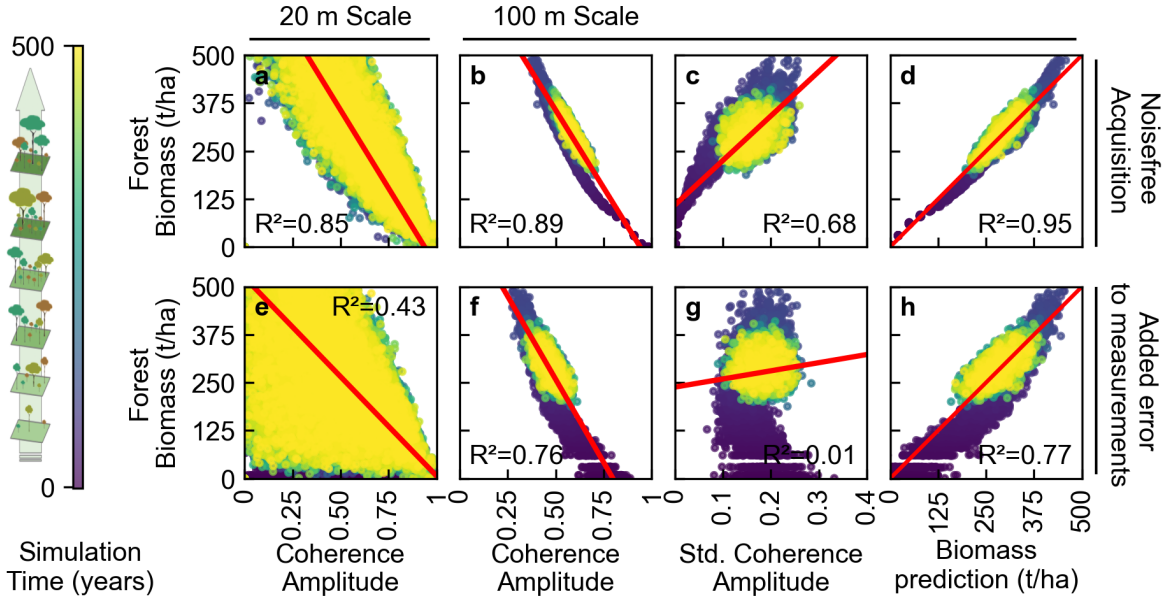

Figure 4. Biomass prediction from different radar coherence metrics for a tropical forest in Panama (BCI, 50 ha). Top row: Above-ground biomass prediction from radar coherence amplitude. (a) 20m resolution linear prediction at the effective TanDEM-X resolution, (b) 100m resolution average (mean), capturing ha-scale properties,(c) 100m standard deviation (std) capturing local variability, (d) 100m bilinear combining mean and std. Bottom row: Impact of 20% measurement noise on the different scenarios (e,f,g,h) compared to the top row. Results based on 100 ha of simulated tropical forest using FORMIND with colors according to simulation time. Red lines indicate respective statistical prediction models (cf. Appendix B). Utilizing spatial aggregation, prediction accuracy can be retained despite the loss due to generalized measurement noise.

3 Results

3.1 Predicting biomass from forest structure derived radar coherence

Using FORMIND-simulated forest structures across successional stages, we investigated how structure-dependent radar coherence enables biomass prediction. We also investigated how measurement noise and spatial scale influence biomass predictions.

Figure 4 illustrates the performance of four AGB regression models based on structure-derived coherence magnitude, comparing predictions at 20m and 100m resolutions. The top row (a-d) presents results in a noiseless scenario, while the bottom row (e-h) shows the impact of 20% noise. The color gradient in each plot represents forest age, tracking the ecosystem's development through successional stages. Measurement errors most severely impact 20 m scale predictions (Fig. 4e), but aggregating to the 100 m plot scale substantially recovers accuracy (Fig. 4f-h). At this coarser scale, mean coherence amplitude emerges as the strongest predictor, while the standard deviation as a metric for plot-level heterogeneity retains some predictive power. A

https://doi.org/10.5194/egusphere-2026-613
Preprint. Discussion started: 16 March 2026

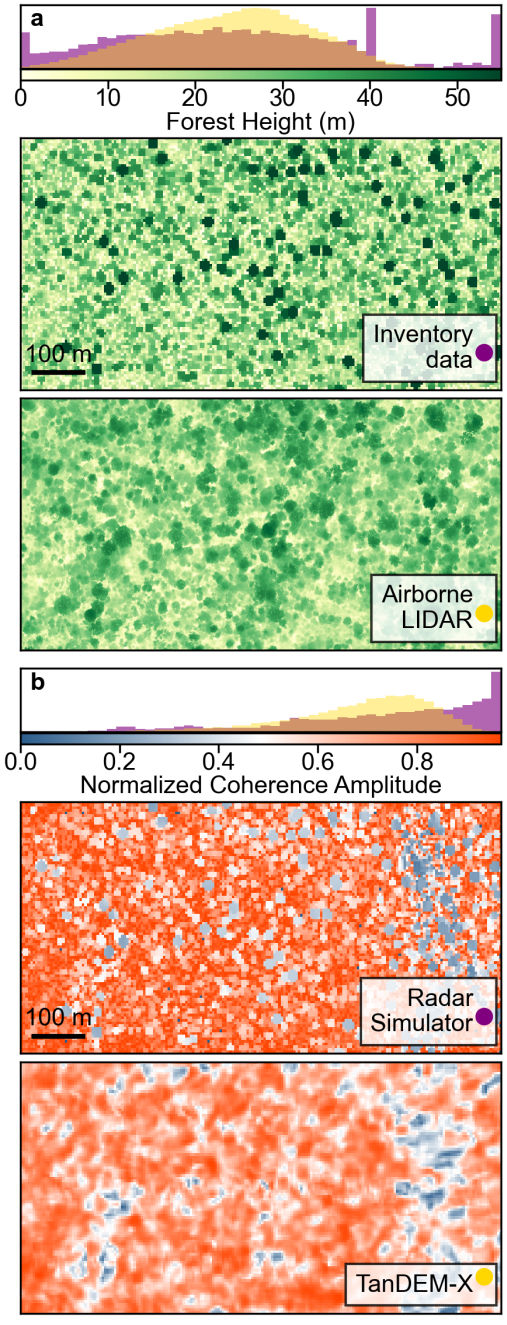

Figure 5. Forest height and radar coherence amplitude for tropical forest in Panama, BCI (50 ha, 5 m resolution). (a) FORMIND canopy height model vs ALS measurements. (b) Radar coherence amplitude (derived from the forest model and radar simulator, cf. Fig. 2(b)) vs TanDEM-X observations.

https://doi.org/10.5194/egusphere-2026-613
Preprint. Discussion started: 16 March 2026

more detailed analysis of the regression statistics is provided in Appendix B, with further analysis of individual successional stages in Appendix A.

3.2 Forest radar simulation at BCI

Figure 5 compares simulated and observed data at the tropical forest of BCI at a spatial resolution of 5 meters. Height distributions show similar means to ALS, though the model includes more gaps (DBH $\geq 10\,\mathrm{cm}$ threshold) and some overestimation of single large trees. Coherence distributions and maps (simulations with the FORMIND forest model, $50\,\mathrm{ha}$) reveal differences in understory coverage. The modeled forest height derived from inventory data only includes trees above the diameter threshold, resulting in canopy gaps. Simulated coherence values reach 1.0 while observations show a long tail toward low values (mean 0.75), linked to the coarse model resolution at this smallest scale. Additional analysis is provided in Appendix E.

3.3 Inverting forest height at BCI

We evaluated forest height from two inversion approaches (P1 and P2) against ALS data at the one-hectare scale (Fig. 6). The distribution of the 50 forest plots in the tropical forest at BCI (Fig. 6a) shows that both P1 and ALS measurements cluster around a mean height of 35 meters, while P2 shows a lower mean of 30 meters. The 1:1 comparison between P1 and ALS (Fig. 6b) reveals strong correspondence with minimal bias. In contrast, while P2 shows a systematic bias in the height estimates (Fig. 6c), it maintains a strong linear spatial correlation with the ALS data, suggesting that it captures relative height variations across the landscape despite a larger absolute height offset.

Detailed validation statistics comparing both products against ALS data are provided in Appendix C.

4 Discussion

We have demonstrated a novel approach to mechanistically connect tree-level ecological processes to interferometric radar observations. Our proposed framework addresses key challenges in current forest remote sensing: lack of understanding of forest radar retrieval, validation between ecological models and radar observations, and reliance on assessing remote sensing data only based on statistical relations. Integrating FORMIND's local explicit 3D forest structures with interferometric modelling enables robust predictions of height and biomass across different forest types, successional stages, and environmental conditions.

Our analysis demonstrates that appropriate spatial aggregation methods are relevant for robust biomass prediction. Max-sampling at 20m resolution, followed by mean-sampling at 100m plots links tree-scale dynamics to plot-scale properties. The varying biomass prediction performance across successional stages highlights how forest structural complexity affects radar signals. Early successional forests, with simpler vertical structure, show higher prediction accuracy, while mature forests with complex multi-layered canopies present greater challenges. This mechanistic insight can be crucial, e.g. for upcoming missions like ESA-BIOMASS (Carreiras et al., 2017), as it provides a process-based framework for understanding how forest structure affects radar signal interpretation.

https://doi.org/10.5194/egusphere-2026-613
Preprint. Discussion started: 16 March 2026

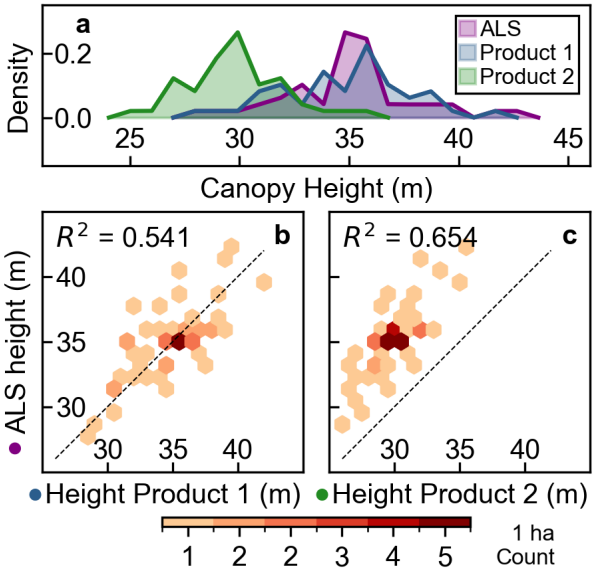

Figure 6. Validation of height inversion approaches. Canopy heights inverted from TanDEM-X vs. Airborne Laser Scanning (ALS) for a tropical forest in Panama, BCI (50 ha), 100 m resolution. (a) Distribution of 50 validation points showing P1 and ALS means at 35m, P2 mean at 30m. (b) The comparison of P1 (coherence amplitude based) with ALS shows a strong correspondence with low bias. (c) In contrast, P2 (coherence amplitude and phase) exhibits a systematic bias but maintains a strong linear correlation with ALS data.

The comparison between simulated and observed coherence distributions at BCI demonstrates both the capabilities and current limitations of our approach. While the model successfully captures general forest structural patterns, discrepancies in canopy densities and subsequently coherence distributions indicate directions for future improvement. Our dual height inversion strategies illustrate the trade-off between absolute accuracy with inversion product P1 and spatial correlation with P2. Resolving the uniform scatterer-assumption in P1 e.g. by locally specific structural indices and the phase-center vs canopy-top mismatch in P2 e.g. by affine debiasing requires further investigation. While our approach represents a significant advance, certain limitations should be acknowledged. The current reliance on DEMs for terrain correction limits applicability in regions without high-quality elevation data.

A common approach for forest remote sensing with single-pass TanDEM-X interferometry is to first invert forest height using the Random Volume over Ground (RVoG) model and then estimate biomass via allometric scaling. This method has been refined through extensions like incorporating polarimetric information or more detailed ground scattering to improve height retrieval (Kugler et al., 2014; Hojo et al., 2020). Schlund and Boehm (2021) proposed a more direct method, demonstrating a linear relationship between radar coherence and forest height. While effective across multiple sites, the question of how spatial scale influences the coherence-height relationship is not addressed. One limitation of both these allometric and simpler linear models is that they can overlook the structural properties of the forest, which influence the radar signal. Recently, He et al. (2023) incorporated structural effects by analyzing the variability of the interferometric phase, using it as a signal-based proxy

https://doi.org/10.5194/egusphere-2026-613
Preprint. Discussion started: 16 March 2026

for canopy complexity. Whether this canopy complexity proxy agrees with our approach of mechanistically representing the 3D canopy structure is a question for future research. Similarly, they emphasize the utilization of an external Digital Elevation Model (DEM).

Results are presented for a tropical case study and can be transferred across forest ecosystems (boreal to tropical) through ecological parameterization.

Future developments should focus on incorporating additional forest processes such as disturbances from fire, windthrow, and logging. These can significantly affect forest structure and radar signatures and could be facilitated as extensions through the framework's modular design.

Individual based forest models can capture localized relations between forest structure, successional stage and biomass in a condensed manner. Building a mechanistic understanding of forest-radar-interaction on top allows to bridge the gap between insights from local field measurements and large-scale remote sensing observations. Our proposed framework opens new possibilities for global forest ecosystem monitoring and is transferable via ecological parameterization and directly relevant for missions such as ESA BIOMASS. Possible applications include real-time forest change detection (e.g. early warning systems for deforestation) and adaptive management strategies, contributing to more accurate and reliable global carbon accounting.

5 Conclusions

We present a mechanistic framework linking individual-based 3D forest dynamics to interferometric radar observations, enabling ecologically consistent height and biomass prediction across forest successional stages. We showed that, (a) forest modelling can improve radar coherence interpretation through its ability to directly represent the vertical scattering structure of forests, (b) radar simulations can reproduce observed coherence patterns in tropical forests qualitatively and (c) using this approach, forest height can be retrieved from radar coherence - as validated here by ALS. Concluding, the mechanistic coupling of individual-based forest models with InSAR coherence enables biomass and height retrieval beyond empirical allometries, improving robustness across successional stages of forests and under noise.

Code and data availability. The individual-based forest model FORMIND used in this study is available at https://formind.org/downloads/ under open terms. The generated dataset of X-band coherence values for forest structural states along the succession of 100 ha of tropical forest in BCI can be retrieved from Zenodo https://doi.org/10.5281/zenodo.18337307 (Grohmann et al., 2026). The field data for BCI used in this study are managed by the ForestGEO network and can be requested via the ForestGEO data portal http://ctfs.si.edu/datarequest/.

Appendix A: Prediction accuracy across successional stages

We analyzed the simulated coherence amplitude for its AGB prediction performance across three forest successional stages (Fig. A1a) at the 1 ha scale: early (pioneer species), mid (AGB overshoot), and late (equilibrium). At 100-meter scale, the model showed strong predictive ability without noise, though performance declined from early (r=0.99) to late succession (r=0.92).

https://doi.org/10.5194/egusphere-2026-613
Preprint. Discussion started: 16 March 2026

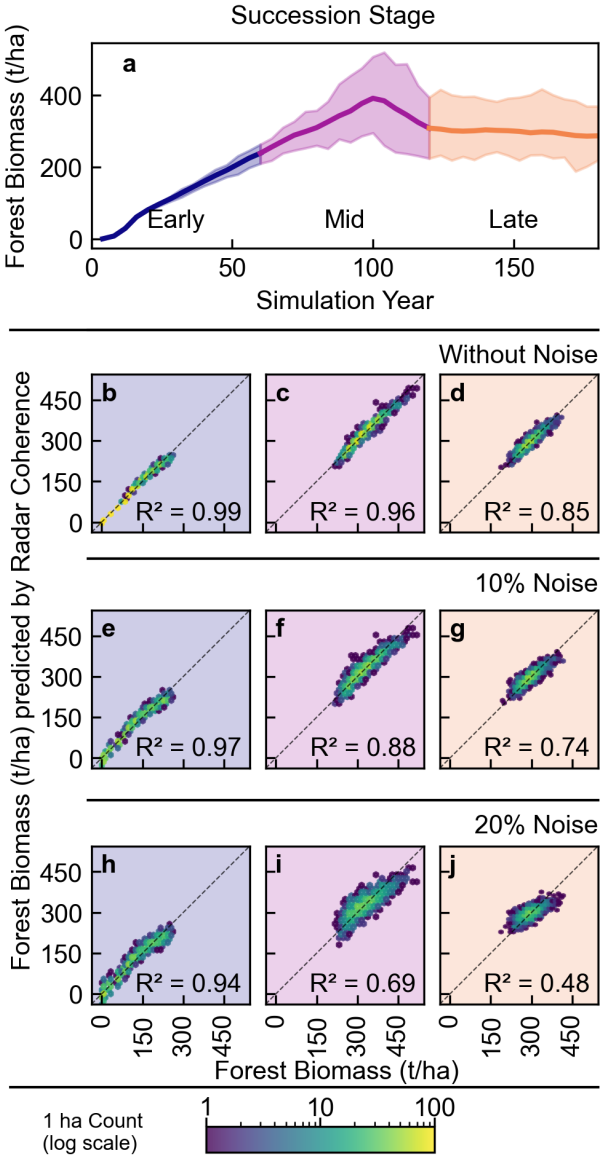

Figure A1. Biomass Prediction accuracy across successional stages and noise levels for tropical forest in Panama, BCI (BCI, 50 ha, 100 m resolution). (a) Aboveground Biomass (AGB) for three successional stages: early (pioneer species), mid (AGB overshoot), and late (equilibrium). Biomass prediction under incremental noise levels: (b-d) original radar Simulations, (e-g) 10%, (h-j) 20% measurement noise. Correlation coefficients decrease with both succession stage and noise level.

Adding 10% noise reduced correlations to 0.98 (early) and 0.86 (late), while 20% noise further degraded performance to 0.97 (early) and 0.69 (late).

https://doi.org/10.5194/egusphere-2026-613
Preprint. Discussion started: 16 March 2026

Table A1. Prediction accuracy for aboveground biomass ($t\,ha^{-1}$) by successional stage at 100 m resolution. N = 1,500 points per stage.

Metric	0% Noise	10% Noise	20% Noise
Early Succession			
Correlation (r)	0.99	0.98	0.97
R^2	0.99	0.97	0.94
RMSE ($t\,ha^{-1}$)	7.25	13.60	17.89
MAE ($t\,ha^{-1}$)	5.77	10.88	14.34
Slope	-473.92	-616.23	-570.25
Intercept ($t\,ha^{-1}$)	460.08	563.57	549.85
Mid Succession			
Correlation (r)	0.98	0.94	0.83
R^2	0.96	0.88	0.69
RMSE ($t\,ha^{-1}$)	10.36	18.31	29.00
MAE ($t\,ha^{-1}$)	7.80	14.29	23.13
Slope	-956.80	-975.50	-904.35
Intercept ($t\,ha^{-1}$)	755.36	703.56	616.96
Late Succession			
Correlation (r)	0.92	0.86	0.69
R^2	0.85	0.74	0.48
RMSE ($t\,ha^{-1}$)	12.86	17.05	24.11
MAE ($t\,ha^{-1}$)	10.23	13.49	19.26
Slope	-734.18	-710.78	-572.65
Intercept ($t\,ha^{-1}$)	679.98	622.03	550.86

Appendix B: Detailed Regression Statistics for Biomass Prediction

Table B1 provides comprehensive regression statistics for the AGB prediction models tested in this study. Coherence amplitude $|\gamma|$ was calculated from the patch LAI-profiles at 20 m resolution, corresponding to patch biomass AGB. At 100 m, biomass AGB is accumulated over the corresponding 20 m patches. Coherence amplitude at 20 m is aggregated to 100 m by the average $\text{mean}_{100}(|\gamma|) = 0.04 \sum_1^{25} |\gamma|$ and by the standard deviation $\text{std}_{100}(|\gamma|) = \sum_1^{25} |\gamma| - \text{mean}_1 00(|\gamma|)$ of the corresponding 25 20 m patches per 100 m plot respectively. The models: **20 m Linear:** $AGB = a\,|\gamma| + b$, **100 m Mean:** $AGB = a\,\text{mean}_{100}(|\gamma|) + b$, **100 m Std Dev:** $AGB = a\,\text{std}_{100}(|\gamma|) + b$, **100 m Bilinear:** $AGB = a\,\text{mean}_{100}(|\gamma|) + b\,\text{std}_{100}(|\gamma|) + c$

Regression was done using least-squares. The progression from 20 m to 100 m scale demonstrates the benefits of spatial aggregation. While the 20 m model shows severe degradation under noise (R^2 dropping from 0.85 to 0.43 with 20% noise), the 100 m models maintain much stronger performance, with the bilinear model retaining $R^2 = 0.77$ even under 20% noise. The

https://doi.org/10.5194/egusphere-2026-613
Preprint. Discussion started: 16 March 2026

Table B1. Regression statistics for biomass models across noise levels ($t\,ha^{-1}$). Sample sizes: 20 m resolution model (N=312,500), 100 m resolution models (N=12,500 each).

Model	Metric	Noise Level		
		0%	10%	20%
20 m Linear	R^2	0.85	0.68	0.43
	RMSE	57.84	84.58	113.07
	MAE	43.89	61.72	83.12
	Slope	-814.23	-725.28	-516.94
	Intercept	763.97	667.23	523.83
100 m Mean	R^2	0.89	0.85	0.76
	RMSE	23.38	27.10	34.39
	MAE	17.41	20.90	26.83
	Slope	-809.47	-861.97	-865.64
	Intercept	761.12	740.94	690.92
100 m Std Dev	R^2	0.68	0.34	0.01
	RMSE	39.73	57.31	70.20
	MAE	30.71	39.96	44.87
	Slope	1159.91	1249.93	212.04
	Intercept	109.56	84.66	238.18
100 m Bilinear	R^2	0.95	0.90	0.77
	RMSE	16.35	22.74	34.05
	MAE	13.16	17.98	26.52
	Slope mean	-612.95	-770.27	-864.52
	Slope std	463.32	496.80	175.24
	Intercept	576.83	615.40	659.04

bilinear model's dual slopes (-864.52 for mean coherence, $+175.24$ for standard deviation) indicate that higher mean coherence correlates with lower biomass (consistent with signal penetration theory), while higher coherence variability correlates with higher biomass (reflecting structural complexity).

Appendix C: Comparative Statistics: TanDEM-X Height inversion vs ALS

Table C1 shows validation statistics comparing TanDEM-X inversions against ALS for forest height. Product P1 achieves superior absolute accuracy (bias: -0.21m, RMSE: 2.10m) while Product P2 shows stronger spatial correlation (r=0.81 vs r=0.74) despite systematic underestimation (-5.29m bias).

https://doi.org/10.5194/egusphere-2026-613
Preprint. Discussion started: 16 March 2026

Table C1. Validation statistics for height inversion products (m) against ALS data for 50 samples at 100 m resolution. Mean ALS Height 35.04 m.

Metric	Product P1	Product P2
Mean Estimated Height (m)	34.83	29.75
Bias (m)	-0.21	-5.29
Relative Bias (%)	-0.60	-15.09
Std-Dev Difference (m)	2.09	1.70
RMSE (m)	2.10	5.55
MAE (m)	1.60	5.29
Normalised RMSE (%)	5.98	15.84
R^2	0.54	0.65
Pearson's r	0.74	0.81
Slope	0.74	0.60
Intercept (m)	9.02	8.63

Table D1. Key TanDEM-X acquisition parameters for the BCI case study: nominal κ_z and incidence angle.

Date	κ_z (rad/m)	θ (°)
2015-10-15	0.09	33.7
2015-10-26	0.09	33.7
2018-03-13	0.11	33.7
2020-01-24	0.12	33.7

Appendix D: Acquisition parameters

The TanDEM-X acquisition parameters significantly influence the sensitivity of coherence measurements to forest structure. The vertical wavenumber κ_z determines the vertical resolution of the interferometric measurement, with higher values providing better sensitivity to canopy structure but reduced penetration depth.

Multiple TanDEM-X acquisitions with varying orbital configurations were used for the BCI case study. Table D1 shows the key acquisition parameters.

Phases are calibrated manually relative to beach level at the BCI coast.

Appendix E: Radar simulation at BCI

Figure E1 shows the framework's forward test at BCI aggregated (mean-average) to 20 m and 100 m resolution. Fig. E1a shows the inventory data based FORMIND canopy height model vs. ALS measurements. While the distributions generally overlap, the

https://doi.org/10.5194/egusphere-2026-613
Preprint. Discussion started: 16 March 2026

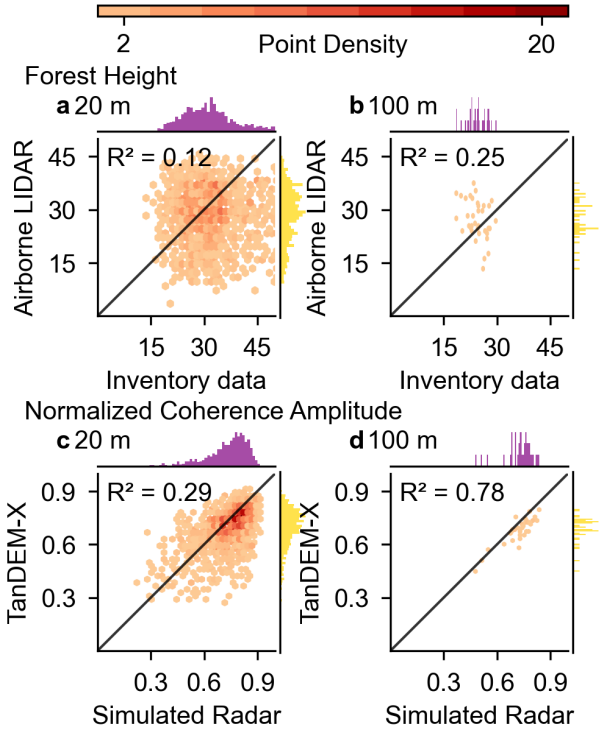

Figure E1. Forest height and radar coherence amplitude at BCI. Data from the displays at Fig. 5 aggregated to 20 m and 100 m resolution. (a-b) Forest heights derived from inventory data processed by FORMIND model vs. ALS measurements. (c-d) Simulated coherence amplitude vs. TanDEM-X observations.

one-to-one correspondence shows discrepancies at this individual-tree-level. Fig. E1b shows the simulated coherence amplitude vs. TanDEM-X observations. While the distributions display similar behavior, the one-to-one correspondence is characterized by agreement in the regime of high coherence amplitude values.

Author contributions. LG conducted the data analysis and simulation. LA and KP processed the InSAR data and provided methodological insights. AH provided conceptualization, administration and funding acquisition. LG wrote the manuscript, and AH, LA, and KP revised the manuscript. All authors approved the manuscript.

Competing interests. The authors declare that they have no known competing financial interests or personal relationships that could have appeared to influence the work reported in this paper.

https://doi.org/10.5194/egusphere-2026-613
Preprint. Discussion started: 16 March 2026

Acknowledgements. This work was supported by the German Ministry of Economics and Climate Protection under grant number [50EE2310]. We thank the Smithsonian Tropical Research Institute for providing access to the Barro Colorado Island Forest Dynamics Plot data. We are grateful to the German Aerospace Center (DLR) for providing TanDEM-X data.

https://doi.org/10.5194/egusphere-2026-613
Preprint. Discussion started: 16 March 2026

References

Armstrong, A., Fischer, R., Huth, A., Shugart, H., and Fatoyinbo, T.: Simulating Forest Dynamics of Lowland Rainforests in Eastern Madagascar, Forests, 9, 214, https://doi.org/10.3390/f9040214, 2018.

Bamler, R. and Hartl, P.: TOPICAL REVIEW: Synthetic aperture radar interferometry, Inverse Problems, 14, 1, https://doi.org/10.1088/0266-5611/14/4/001, 1998.

Bauer, L., Knapp, N., and Fischer, R.: Mapping Amazon Forest Productivity by Fusing GEDI Lidar Waveforms with an Individual-Based Forest Model, Remote Sensing, 13, 4540, https://doi.org/10.3390/rs13224540, 2021.

Burns, P., Hakkenberg, C. R., and Goetz, S. J.: Multi-resolution gridded maps of vegetation structure from GEDI, Scientific Data, 11, 881, https://doi.org/10.1038/s41597-024-03668-4, 2024.

Carreiras, J. M., Quegan, S., Le Toan, T., Ho Tong Minh, D., Saatchi, S. S., Carvalhais, N., Reichstein, M., and Scipal, K.: Coverage of high biomass forests by the ESA BIOMASS mission under defense restrictions, Remote Sensing of Environment, 196, 154–162, https://doi.org/10.1016/j.rse.2017.05.003, 2017.

Chave, J., Condit, R., Lao, S., Caspersen, J. P., Foster, R. B., and Hubbell, S. P.: Spatial and temporal variation of biomass in a tropical forest: results from a large census plot in Panama, Journal of Ecology, 91, 240–252, https://doi.org/10.1046/j.1365-2745.2003.00757.x, 2003.

Cherrington, E. A., Evans, C. A., Limaye, A. S., Anderson, E. R., and Flores-Anderson, A. I.: Reviews and syntheses: One forest carbon model to rule them all? Utilizing ensembles of forest cover and biomass datasets to determine carbon budgets of the world's forest ecosystems, https://doi.org/10.5194/egusphere-2024-1179, 2024.

Choi, C., Cazcarra-Bes, V., Guliaev, R., Pardini, M., Papathanassiou, K. P., Qi, W., Armston, J., and Dubayah, R. O.: Large-Scale Forest Height Mapping by Combining TanDEM-X and GEDI Data, IEEE Journal of Selected Topics in Applied Earth Observations and Remote Sensing, 16, 2374–2385, https://doi.org/10.1109/JSTARS.2023.3244866, 2023.

Condit, R., Chisholm, R. A., and Hubbell, S. P.: Thirty Years of Forest Census at Barro Colorado and the Importance of Immigration in Maintaining Diversity, PLoS ONE, 7, e49 826, https://doi.org/10.1371/journal.pone.0049826, 2012a.

Condit, R., Lao, S., Pérez, R., Dolins, S. B., Foster, R. B., and Hubbell, S. P.: Barro Colorado Forest Census Plot Data, 50 ha, Version 2012, https://doi.org/10.5479/data.bci.20130603, 2012b.

Dubayah, R., Armston, J., Healey, S. P., Bruening, J. M., Patterson, P. L., Kellner, J. R., Duncanson, L., Saarela, S., Ståhl, G., Yang, Z., Tang, H., Blair, J. B., Fatoyinbo, L., Goetz, S., Hancock, S., Hansen, M., Hofton, M., Hurtt, G., and Luthcke, S.: GEDI launches a new era of biomass inference from space, Environmental Research Letters, 17, 095 001, https://doi.org/10.1088/1748-9326/ac8694, 2022.

Feeley, K. J., Davies, S. J., Perez, R., Hubbell, S. P., and Foster, R. B.: Directional changes in the species composition of a tropical forest, Ecology, 92, 871–882, https://doi.org/10.1890/10-0724.1, 2011.

Fischer, R., Bohn, F., Dantas De Paula, M., Dislich, C., Groeneveld, J., Gutiérrez, A. G., Kazmierczak, M., Knapp, N., Lehmann, S., Paulick, S., Pütz, S., Rödig, E., Taubert, F., Köhler, P., and Huth, A.: Lessons learned from applying a forest gap model to understand ecosystem and carbon dynamics of complex tropical forests, Ecological Modelling, 326, 124–133, https://doi.org/10.1016/j.ecolmodel.2015.11.018, 2016.

Fischer, S. M., Wang, X., and Huth, A.: Distinguishing mature and immature trees allows estimating forest carbon uptake from stand structure, Biogeosciences, 21, 3305–3319, https://doi.org/10.5194/bg-21-3305-2024, 2024.

Grohmann, L., Albrecht, L., Papathanassiou, K., and Huth, A.: Linking Individual-Based Forest Models with Radar Simulation: Data and Code, https://doi.org/10.5281/zenodo.18337307, 2026.

https://doi.org/10.5194/egusphere-2026-613
Preprint. Discussion started: 16 March 2026

Harris, N. L., Gibbs, D. A., Baccini, A., Birdsey, R. A., De Bruin, S., Farina, M., Fatoyinbo, L., Hansen, M. C., Herold, M., Houghton, R. A., Potapov, P. V., Suarez, D. R., Roman-Cuesta, R. M., Saatchi, S. S., Slay, C. M., Turubanova, S. A., and Tyukavina, A.: Global maps of twenty-first century forest carbon fluxes, Nature Climate Change, 11, 234–240, https://doi.org/10.1038/s41558-020-00976-6, 2021.

He, W., Zhu, J., Lopez-Sanchez, J. M., Gómez, C., Fu, H., and Xie, Q.: Forest Height Inversion by Combining Single-Baseline TanDEM-X InSAR Data with External DTM Data, Remote Sensing, 15, 5517, https://doi.org/10.3390/rs15235517, 2023.

Henniger, H., Bohn, F. J., Schmidt, K., and Huth, A.: A New Approach Combining a Multilayer Radiative Transfer Model with an Individual-Based Forest Model: Application to Boreal Forests in Finland, Remote Sensing, 15, 3078, https://doi.org/10.3390/rs15123078, 2023.

Hiltner, U., Huth, A., Hérault, B., Holtmann, A., Bräuning, A., and Fischer, R.: Climate change alters the ability of neotropical forests to provide timber and sequester carbon, Forest Ecology and Management, 492, 119 166, https://doi.org/10.1016/j.foreco.2021.119166, 2021.

Hojo, A., Takagi, K., Avtar, R., Tadono, T., and Nakamura, F.: Synthesis of L-Band SAR and Forest Heights Derived from TanDEM-X DEM and 3 Digital Terrain Models for Biomass Mapping, Remote Sensing, 12, 349, https://doi.org/10.3390/rs12030349, publisher: MDPI AG, 2020.

Hubbell, S. P.: Tropical rain forest conservation and the twin challenges of diversity and rarity, Ecology and Evolution, 3, 3263–3274, https://doi.org/10.1002/ece3.705, 2013.

Knapp, N., Fischer, R., and Huth, A.: Linking lidar and forest modeling to assess biomass estimation across scales and disturbance states, Remote Sensing of Environment, 205, 199–209, https://doi.org/10.1016/j.rse.2017.11.018, 2018.

Knapp, N., Fischer, R., Cazcarra-Bes, V., and Huth, A.: Structure metrics to generalize biomass estimation from lidar across forest types from different continents, Remote Sensing of Environment, 237, 111 597, https://doi.org/10.1016/j.rse.2019.111597, 2020.

Kugler, F., Schulze, D., Hajnsek, I., Pretzsch, H., and Papathanassiou, K. P.: TanDEM-X Pol-InSAR Performance for Forest Height Estimation, IEEE Transactions on Geoscience and Remote Sensing, 52, 6404–6422, https://doi.org/10.1109/tgrs.2013.2296533, publisher: Institute of Electrical and Electronics Engineers (IEEE), 2014.

Köhler, P. and Huth, A.: The effects of tree species grouping in tropical rainforest modelling: Simulations with the individual-based model Formind, Ecological Modelling, 109, 301–321, https://doi.org/10.1016/S0304-3800(98)00066-0, 1998.

Lang, N., Jetz, W., Schindler, K., and Wegner, J. D.: A high-resolution canopy height model of the Earth, Nature Ecology & Evolution, 7, 1778–1789, https://doi.org/10.1038/s41559-023-02206-6, 2023.

Lorey, T.: Die Bestimmung der mittleren Querschnittsfläche von Waldbeständen, Allgemeine Forst- und Jagdzeitung, 63, 497–511, 1887.

Mascaro, J., Asner, G. P., Muller-Landau, H. C., Van Breugel, M., Hall, J., and Dahlin, K.: Controls over aboveground forest carbon density on Barro Colorado Island, Panama, https://doi.org/10.5194/bgd-7-8817-2010, 2010.

Meyer, V., Saatchi, S. S., Chave, J., Dalling, J. W., Bohlman, S., Fricker, G. A., Robinson, C., Neumann, M., and Hubbell, S.: Detecting tropical forest biomass dynamics from repeated airborne lidar measurements, Biogeosciences, 10, 5421–5438, https://doi.org/10.5194/bg-10-5421-2013, 2013.

Mo, L., Zohner, C. M., Reich, P. B., Liang, J., De Miguel, S., Nabuurs, G.-J., Renner, S. S., Van Den Hoogen, J., Araza, A., Herold, M., Mirzagholi, L., Ma, H., Averill, C., Phillips, O. L., Gamarra, J. G. P., Hordijk, I., Routh, D., Abegg, M., Adou Yao, Y. C., Alberti, G., Almeyda Zambrano, A. M., Alvarado, B. V., Alvarez-Dávila, E., Alvarez-Loayza, P., Alves, L. F., Amaral, I., Ammer, C., Antón-Fernández, C., Araujo-Murakami, A., Arroyo, L., Avitabile, V., Aymard, G. A., Baker, T. R., Bałazy, R., Banki, O., Barroso, J. G., Bastian, M. L., Bastin, J.-F., Birigazzi, L., Birnbaum, P., Bitariho, R., Boeckx, P., Bongers, F., Bouriaud, O., Brancalion, P. H. S., Brandl, S., Brearley, F. Q., Brienen, R., Broadbent, E. N., Bruelheide, H., Bussotti, F., Cazzolla Gatti, R., César, R. G., Cesljar, G., Chazdon, R. L., Chen, H. Y. H., Chisholm, C., Cho, H., Cienciala, E., Clark, C., Clark, D., Colletta, G. D., Coomes, D. A., Cornejo Valverde, F.,

https://doi.org/10.5194/egusphere-2026-613
Preprint. Discussion started: 16 March 2026

Corral-Rivas, J. J., Crim, P. M., Cumming, J. R., Dayanandan, S., De Gasper, A. L., Decuyper, M., Derroire, G., DeVries, B., Djordjevic, I., Dolezal, J., Dourdain, A., Engone Obiang, N. L., Enquist, B. J., Eyre, T. J., Fandohan, A. B., Fayle, T. M., Feldpausch, T. R., Ferreira, L. V., Finér, L., Fischer, M., Fletcher, C., Frizzera, L., Gianelle, D., Glick, H. B., Harris, D. J., Hector, A., Hemp, A., Hengeveld, G., Hérault, B., Herbohn, J. L., Hillers, A., Honorio Coronado, E. N., Hui, C., Ibanez, T., Imai, N., Jagodziński, A. M., Jaroszewicz, B., Johannsen, V. K., Joly, C. A., Jucker, T., Jung, I., Karminov, V., Kartawinata, K., Kearsley, E., Kenfack, D., Kennard, D. K., Kepfer-Rojas, S., Keppel, G., Khan, M. L., Killeen, T. J., Kim, H. S., Kitayama, K., Köhl, M., Korjus, H., Kraxner, F., Kucher, D., Laarmann, D., Lang, M., Lu, H., Lukina, N. V., Maitner, B. S., Malhi, Y., Marcon, E., Marimon, B. S., Marimon-Junior, B. H., Marshall, A. R., Martin, E. H., Meave, J. A., Melo-Cruz, O., Mendoza, C., Mendoza-Polo, I., Miscicki, S., Merow, C., Monteagudo Mendoza, A., Moreno, V. S., Mukul, S. A., Mundhenk, P., Nava-Miranda, M. G., Neill, D., Neldner, V. J., Nevenic, R. V., Ngugi, M. R., Niklaus, P. A., Oleksyn, J., Ontikov, P., Ortiz-Malavasi, E., Pan, Y., Paquette, A., Parada-Gutierrez, A., Parfenova, E. I., Park, M., Parren, M., Parthasarathy, N., Peri, P. L., Pfautsch, S., Picard, N., Piedade, M. T. F., Piotto, D., Pitman, N. C. A., Poulsen, A. D., Poulsen, J. R., Pretzsch, H., Ramirez Arevalo, F., Restrepo-Correa, Z., Rodeghiero, M., Rolim, S. G., Roopsind, A., Rovero, F., Rutishauser, E., Saikia, P., Salas-Eljatib, C., Saner, P., Schall, P., Schelhaas, M.-J., Schepaschenko, D., Scherer-Lorenzen, M., Schmid, B., Schöngart, J., Searle, E. B., Seben, V., Serra-Diaz, J. M., Sheil, D., Shvidenko, A. Z., Silva-Espejo, J. E., Silveira, M., Singh, J., Sist, P., Slik, F., Sonké, B., Souza, A. F., Stereńczak, K. J., Svenning, J.-C., Svoboda, M., Swanepoel, B., Targhetta, N., Tchebakova, N., Ter Steege, H., Thomas, R., Tikhonova, E., Umunay, P. M., Usoltsev, V. A., Valencia, R., Valladares, F., Van Der Plas, F., Van Do, T., Van Nuland, M. E., Vasquez, R. M., Verbeeck, H., Viana, H., Vibrans, A. C., Vieira, S., Von Gadow, K., Wang, H.-F., Watson, J. V., Werner, G. D. A., Wiser, S. K., Wittmann, F., Woell, H., Wortel, V., Zagt, R., Zawiła-Niedźwiecki, T., Zhang, C., Zhao, X., Zhou, M., Zhu, Z.-X., Zo-Bi, I. C., Gann, G. D., and Crowther, T. W.: Integrated global assessment of the natural forest carbon potential, Nature, 624, 92–101, https://doi.org/10.1038/s41586-023-06723-z, 2023.

Pan, Y., Birdsey, R. A., Fang, J., Houghton, R., Kauppi, P. E., Kurz, W. A., Phillips, O. L., Shvidenko, A., Lewis, S. L., Canadell, J. G., Ciais, P., Jackson, R. B., Pacala, S. W., McGuire, A. D., Piao, S., Rautiainen, A., Sitch, S., and Hayes, D.: A Large and Persistent Carbon Sink in the World's Forests, Science, 333, 988–993, https://doi.org/10.1126/science.1201609, 2011.

Papathanassiou, K. and Cloude, S.: Single-baseline polarimetric SAR interferometry, IEEE Transactions on Geoscience and Remote Sensing, 39, 2352–2363, https://doi.org/10.1109/36.964971, 2001.

Rödig, E., Cuntz, M., Rammig, A., Fischer, R., Taubert, F., and Huth, A.: The importance of forest structure for carbon fluxes of the Amazon rainforest, Environmental Research Letters, 13, 054 013, https://doi.org/10.1088/1748-9326/aabc61, 2018.

Rödig, E., Knapp, N., Fischer, R., Bohn, F. J., Dubayah, R., Tang, H., and Huth, A.: From small-scale forest structure to Amazon-wide carbon estimates, Nature Communications, 10, 5088, https://doi.org/10.1038/s41467-019-13063-y, 2019.

Schlund, M. and Boehm, H. D. V.: Assessment of linear relationships between TanDEM-X coherence and canopy height as well as aboveground biomass in tropical forests, International Journal of Remote Sensing, 42, 3405–3425, https://doi.org/10.1080/01431161.2020.1871101, publisher: Informa UK Limited, 2021.

Tietjen, B. and Huth, A.: Modelling dynamics of managed tropical rainforests—An aggregated approach, Ecological Modelling, 199, 421–432, https://doi.org/10.1016/j.ecolmodel.2005.11.045, 2006.

Treuhaft, R. N. and Siqueira, P. R.: Vertical structure of vegetated land surfaces from interferometric and polarimetric radar, Radio Science, 35, 141–177, https://doi.org/10.1029/1999RS900108, 2000.

Treuhaft, R. N., Madsen, S. N., Moghaddam, M., and Van Zyl, J. J.: Vegetation characteristics and underlying topography from interferometric radar, Radio Science, 31, 1449–1485, https://doi.org/10.1029/96RS01763, 1996.

https://doi.org/10.5194/egusphere-2026-613
Preprint. Discussion started: 16 March 2026

Zhang, Y., Zou, Y., and Wang, Y.: Remote Sensing of Forest Above-Ground Biomass Dynamics: A Review, Forests, 16, 821, https://doi.org/10.3390/f16050821, 2025.

Zhao, X., Liu, J., Hao, H., and Yang, Y.: Quantifying the Spatial Heterogeneity and Driving Factors of Aboveground Forest Biomass in the Urban Area of Xi'an, China, ISPRS International Journal of Geo-Information, 9, 744, https://doi.org/10.3390/ijgi9120744, 2020.

Zink, M., Krieger, G., Fiedler, H., and Moreira, A.: The TanDEM-X mission: Overview and status, in: 2007 IEEE International Geoscience and Remote Sensing Symposium, pp. 3944–3947, IEEE, Barcelona, Spain, ISBN 978-1-4244-1211-2, https://doi.org/10.1109/IGARSS.2007.4423711, 2007.